

PACS numbers: 42.60.Fc; 42.55.Px
DOI: 10.1070/QE2006v036n11ABEH013221

Mode locking of an external cavity asymmetric quantum-well GaAs/AlGaAs semiconductor laser

P.P. Vasil'ev, H. Kan, H. Ohta, T. Hiruma, K. Tanaka

***Abstract*. A theoretical model of the optical gain in asymmetric GaAs/AlGaAs quantum-well lasers is developed. It is demonstrated that the emission spectrum of asymmetric GaAs/AlGaAs quantum-well lasers is much broader than that of standard quantum-well lasers. The experimental samples of such lasers and superluminescent diodes with the emission bandwidth exceeding 50 nm are fabricated. Wavelength tunable ultrashort pulses with duration of 1 – 2 ps at repetition rates of 0.4 – 1 GHz are obtained by active mode locking of an external cavity laser.**

Keywords: *mode locking, quantum wells, external cavity*.

1. Introduction

The generation of ultrashort optical pulses is one of the most promising and attractive fields of quantum electronics. Modern mode-locked solid-state lasers can generate optical pulses as short as a few femtoseconds, which is comparable with one oscillation cycle in the optical spectrum range. At the same time, semiconductor lasers, which seemed very promising for the generation of ultrashort pulses at the beginning of the laser era, at present leg behind strongly in respect of duration of generated pulses compared to solid-state lasers [1].

In our opinion, this is caused by two main factors. First, the bandwidth of the optical gain in semiconductor lasers is narrower by a few times than that of solid-state lasers. Second, due to a low power level of semiconductor lasers, media with large nonlinear coefficients suitable for semiconductor absorber mirrors (SESAMs) have not been found yet. Kerr-type mode locking has not been realised in semiconductor lasers so far.

One of the most promising methods of increasing the emission bandwidth of a semiconductor laser is the use of asymmetric quantum-well (AQW) structures [2]. Such lasers contain a few QWs having different widths and/or compositions. The energy diagram of an AQW structure consisting of four QWs, is schematically shown in Fig. 1. Because energy levels in a QW depend both on the composition and width, the levels in the asymmetric structure are distributed in a wide spectral range. This means that the total optical gain has a much wider spectral bandwidth compared to the gain from each QW or from a set of identical QWs. In addition, it is possible to obtain the gain profile with the flat top in a relatively broad spectral range by choosing properly the widths and compositions of QWs.

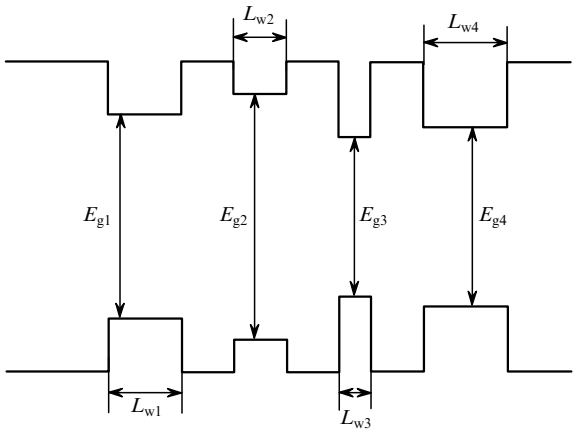

Figure 1. Energy diagram of an AQW structure consisting of four QWs.

Semiconductor lasers based on AQWs are used to generate single-frequency emission tunable in a broad spectral range [3 – 6]. In this case, a laser is placed in an external dispersive resonator with a reflecting diffraction grating. The emission line tuning over 170 nm near 1.55 μm was obtained in such InGaAsP heterostructure laser [7].

Unlike the above-mentioned papers, our goal is to use AQW lasers for the generation of ultrashort pulses. The larger emission bandwidths of such lasers ensure the generation of shorter pulses, which can be tuned in a broad spectral range [8].

One of the main problems in the development of AQW lasers is a proper selection of the width and composition of each well. A theoretical model of the gain in the structure is usually constructed for this purpose [5, 9 – 12]. In this paper, we start with the development of the theoretical model. The theoretical calculation of the optical gain in a QW structure, which consists of two – four QWs of different widths and compositions, is presented in Section 2. Section 3 is devoted to the study of main properties of experimental samples of

P.P. Vasil'ev P.N. Lebedev Physics Institute, Russian Academy of Sciences, Leninsky prosp. 53, 119991 Moscow, Russia;
email: peter@sci.lebedev.ru;
H. Kan, H. Ohta, T. Hiruma, K. Tanaka Central Research Laboratory, Hamamatsu Photonics K.K., 5000 Hirakuchi, Hamamatsu City, 434-8601 Japan

Received 15 May 2006; revision received 8 August 2006
Kvantovaya Elektronika **36** (11) 1065 – 1071 (2006)
Translated by P.P. Vasil'ev

lasers fabricated based on the calculations. The results of the study of active mode locking in an external cavity laser are presented in Section 4.

2. Calculation of the gain of an AQW structure

To construct a theoretical model and optimise the parameters of AQW structures, we used the approach developed in [5, 9–12]. The optical gain spectrum and its dependence on the pump current are the two important parameters that are required for the development of QW lasers and improvement of their characteristics. The optical gain spectrum is calculated, as a rule, by two methods. In the first method analythic expressions are obtained for the optical gain itself. This method requires minimal numerical calculations; however, its application is considerably restricted due to limitations introduced in the derivation of analytic expressions. The second approach is based on numerical methods, when all the parameters are calculated without preliminary simplifications, which allows the calculations of various AQW combinations. We used the second approach. The simulation was performed for electrically neutral QWs in the case of the dynamic equilibrium of carriers in the subbands of different wells and, hence, for the same Fermi levels in all the wells.

For simplicity, we assume that the total gain in the structure is a sum of gains of each QW

$$G(\hbar\omega) = \sum_i G_i(\hbar\omega). \tag{1}$$

Due to a small thickness of the active layer of the laser, optical emission is not localised in it completely. This is taken into account with the help of the optical confinement factor Γ. Because the widths of QWs can be different, the confinement factors for different wells are also different. Then the modal gain of ith QW is given by

$$G_i(\hbar\omega) = \Gamma_i g_i(\hbar\omega), \tag{2}$$

where $g_i(\hbar\omega)$ is the material gain of ith QW.

To calculate the material gain in each QW, first the energy diagram of the structure is constructed. Figure 2 shows schematically the diagram of a QW. The energy diagram of the whole structure is constructed by calculating the band gap for each part of the structure. The band gap of two-component solid $Al_xGa_{1-x}As$ solutions is calculated by using well-known expressions. Then, the energy levels E_{c1}, E_{c2}, ..., E_{cn}, E_{v1}, E_{v2}, ..., E_{vn} of electrons and holes in QWs are determined by solving the one-dimensional Schrödinger equation in the effective mass approximation. At this stage, rather large widths of the barriers between QWs were taken at which the influence of one QW on another was weak. This simplification allows the calculation of the energy levels in each QW separately rather than for the entire structure.

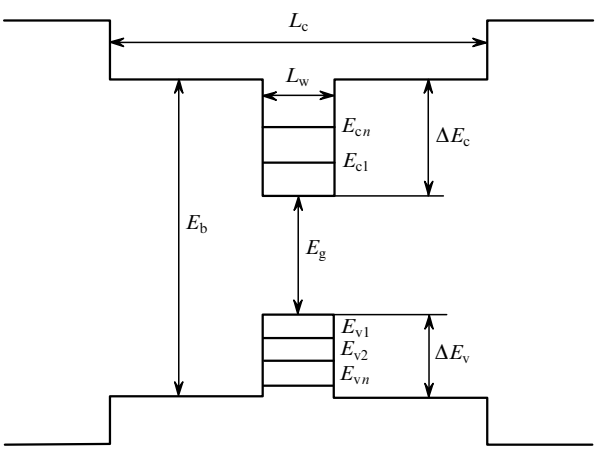

Figure 2. Zone diagram of a QW showing the energy levels and notations used in the numerical model.

After simple calculations [13] we obtain the transcendent equation for the calculation of the electronic energy levels in the QW:

$$\frac{L_w\sqrt{2m_cE}}{\hbar} - \pi n = \arctan\frac{\sqrt{m_cE}/\sqrt{m_{bc1}}}{\sqrt{\Delta E_{c1} - E}} + \arctan\frac{\sqrt{m_cE}/\sqrt{m_{bc2}}}{\sqrt{\Delta E_{c2} - E}}, \tag{3}$$

where L_w is the well width; m_c is the electron effective mass in the QW; m_{bc1} is the electron effective mass in the left barrier; m_{bc2} is the electron effective mass in the right barrier; ΔE_{c1} is height of the barrier on the left; ΔE_{c2} is height of the barrier on the right; E is the energy of the particle. The equation for the hole levels is similar.

The carrier distribution among different quantum states is then determined for the calculation of the optical gain. For this purpose, the number of possible quantum states of electrons and holes is determined and actual distribution among these quantum states is found. The first part of this problem consists in the calculation of the density of states in a QW and above it, and the second part involves the determination of Fermi quasi-levels for electrons and light and heavy holes.

The optical gain in the QW can be written in the form [14]

$$g_{qw}(\hbar\omega, E) = \frac{\pi e^2}{m_0^2\varepsilon_0 c\omega n^2}\sum_{n_c}\sum_{n_v}\rho(E)M^2(E)(f_c - f_v), \tag{4}$$

where E is energy; $\hbar\omega$ is the photon energy; m_0 is free electron mass; c is the speed of light in vacuum; n is the refractive index of the active medium; M is the dipole matrix element of the interband transition; and f_c and f_v are the Fermi functions in the conduction and valence bands. The sum in (4) is performed over all the energy levels in the valence and conduction bands. The combined density of states in Eqn (4) for transitions with heavy and light holes in the discrete and continuous spectrum is described by the expressions [15]

$$\rho_{lh}(E) = \frac{m_{lh}m_cH(E - E_g - E_{ci} + E_{vlhi})}{\pi\hbar^2L_w(m_c + m_{lh})} \quad \text{for} \quad E < E_{gb}, \tag{5}$$

$$\rho_{lh}(E) = \frac{4\pi}{(2\pi\hbar)^3}\left(\frac{2m_cm_{lh}}{m_c + m_{lh}}\right)^{3/2}\sqrt{E - E_g} \quad \text{for} \quad E > E_{gb}, \tag{6}$$

$$\rho_{hh}(E) = \frac{m_{hh}m_cH(E - E_g - E_{ci} + E_{vhhi})}{\pi\hbar^2L_w(m_c + m_{hh})} \quad \text{for} \quad E < E_{gb}, \tag{7}$$

$$\rho_{\rm hh}(E)=\frac{4\pi}{(2\pi\hbar)^3}\left(\frac{2m_{\rm c}m_{\rm hh}}{m_{\rm c}+m_{\rm hh}}\right)^{3/2}\sqrt{E-E_{\rm g}}\ \text{ for }\ E>E_{\rm gb}, \quad (8)$$

where $H(E)$ is the Heaviside function. The transition matrix elements in QWs involving heavy and light holes are calculated from the expressions [15]

$$M^2_{\rm hh}(E)=\frac{3}{4}M^2_{\rm DH}(E)$$

$$\times\left[1+\frac{E_{{\rm c}i}}{E_{{\rm c}i}+m_{\rm hh}(E-E_{\rm g}-E_{{\rm c}i}+E_{{\rm vhh}i})/(m_{\rm c}+m_{\rm hh})}\right], \quad (9)$$

$$M^2_{\rm lh}(E)=2M^2_{\rm DH}(E)-M^2_{\rm hh}(E), \quad (10)$$

$$M^2_{\rm DH}(E)=\frac{m_0^2E_{\rm g}(E_{\rm g}+\Delta)}{12m_{\rm c}(E_{\rm g}+2\Delta/3)}, \quad (11)$$

where Δ is the spin-orbit energy. The Fermi functions in Eqn (4) are defined as

$$f_{\rm c}=\left\{1+\exp\left[\frac{E_{{\rm c}i}}{kT}+\frac{m_{\rm lh}(E-E_{\rm g}-E_{{\rm c}i}+E_{{\rm vlh}i})}{(m_{\rm c}+m_{\rm lh})kT}-\frac{E_{\rm fc}}{kT}\right]\right\}^{-1}. \quad (12)$$

$$f_{\rm v}=\left\{1+\exp\left[-\frac{E_{{\rm vlh}i}}{kT}+\frac{m_{\rm c}(E-E_{\rm g}-E_{{\rm c}i}+E_{{\rm vlh}i})}{(m_{\rm c}+m_{\rm lh})kT}-\frac{E_{\rm fv}}{kT}\right]\right\}^{-1}. \quad (13)$$

$$f_{\rm c}=\left\{1+\exp\left[\frac{E_{{\rm c}i}}{kT}+\frac{m_{\rm hh}(E-E_{\rm g}-E_{{\rm c}i}+E_{{\rm vhh}i})}{(m_{\rm c}+m_{\rm hh})kT}-\frac{E_{\rm fc}}{kT}\right]\right\}^{-1}. \quad (14)$$

$$f_{\rm v}=\left\{1+\exp\left[-\frac{E_{{\rm vhh}i}}{kT}+\frac{m_{\rm c}(E-E_{\rm g}-E_{{\rm c}i}+E_{{\rm vhh}i})}{(m_{\rm c}+m_{\rm hh})kT}-\frac{E_{\rm fv}}{kT}\right]\right\}^{-1}, \quad (15)$$

where $E_{\rm fc}$ and $E_{\rm fv}$ are the Fermi quasi-levels for electrons and holes, respectively. The gain $g_{\rm 3D}(\hbar\omega,E)$ from the continuous spectrum (above the barrier) is calculated similarly.

The total gain for photons with the energy $\hbar\omega$ is determined by the convolution of the net gain in the QW and above the barrier with the weight function $L(E)$ determining the width of the levels [14]. For simplicity, we present this function by the Lorenzian

$$\mathscr{F}(E)=\frac{1}{\pi}\,\frac{\hbar/\tau_{\rm in}}{(\hbar/\tau_{\rm in})^2+(\hbar\omega-E)^2},$$

where $\tau_{\rm in}$ is the intraband relaxation time.

Then,

$$g(\hbar\omega)=\int[g_{\rm qw}(\hbar\omega,E)+g_{\rm 3D}(\hbar\omega,E)]\mathscr{F}(E)\,{\rm d}E. \quad (16)$$

The optical gain, the carrier concentration, and the threshold current density in the cw lasing regime are determined by the cavity loss α, the cavity length L, and the reflection coefficients of the facets (R_1, R_2) according to the well-known relation

$$R_1R_2\exp\{2[G(\omega)-\alpha]L\}=1. \quad (17)$$

Therefore, it is possible to calculate the carrier density and the optical gain $G(\omega)$ in the stationary regime by using the carrier density and the expressions of the optical gain via the electron and hole concentrations and by solving Eqn (17). Several computer programs have been written for this purpose. The input parameters are the pump current density, the cavity parameters R_1, R_2, α, and L, the parameters of the heterostructure, the number of QWs (from 2 to 4), their widths and composition.

The goal was to select the above-mentioned parameters in such a way that the gain profile $G(\omega)$ would have the maximum possible bandwidth and a top as flat as possible. To optimise the structure, we sorted out a huge amount of values of these parameters. We present here just one example from many others. Figure 3 presents gain profiles in an AQW GaAs/AlGaAs structure for three pump levels. The structure contains four QWs. Their widths are 4, 8, 9, and 15 nm and the band gaps are 1.50, 1.50, 1.60 and 1.42 eV, respectively. The gian bandwidths in Fig. 3 are 19, 27 and 32 nm, which is several times larger than the typical gain bandwidth (8 nm) in a standard QW structure having uniform composition and the same QW width for the same

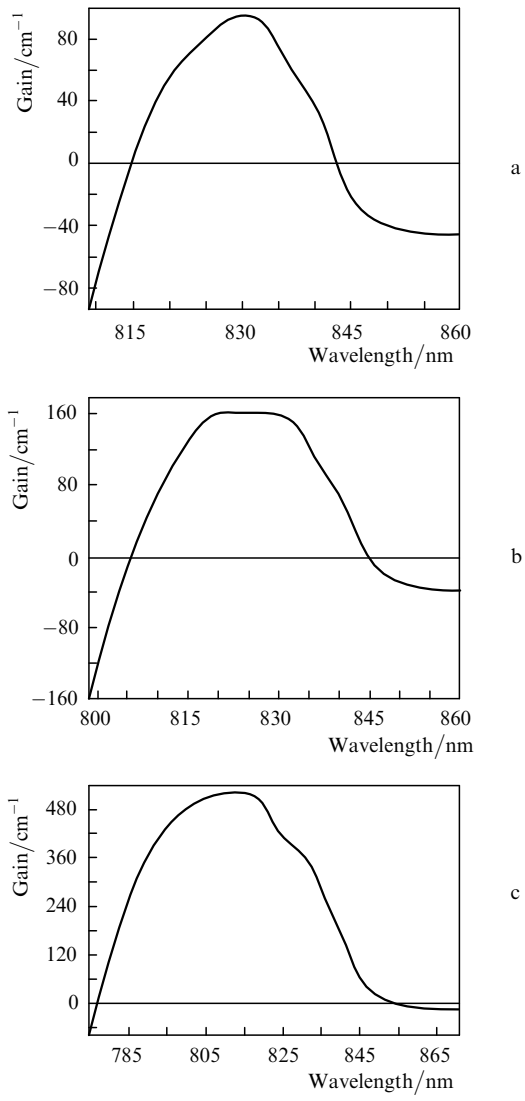

Figure 3. Calculated optical gain spectra of the AQW structure with four QWs for pump levels 429 (a), 479 (b), and 520 A cm^{-2} (c).

pump levels [14]. Figure 3(b) shows that the calculated optical gain profile can have a flat top, but unfortunately, this shape of the gain band exists only within a small range of the pump currents. As the pump current is increased, the gain band is distorted due to the enhancement of the gain from the short-wavelength side corresponding to high-lying energy levels in the QW (Fig. 3c).

3. Characteristics of the experimental samples

Some experimental samples of AQW structures for ultrashort pulse generation were fabricated using the results of calculations described in the previous section. For simplicity, we calculated two QWs for the wavelength range from 810 to 830 nm. The optimum composition and widths of QWs were determined, the latter being 4 and 7.6 nm. The wells were separated by a 15-nm wide barrier. About 20 samples were fabricated and studied. Some of them had a standard waveguide (stripe), which was perpendicular to the chip facets, while the others had inclined waveguides. The width of the waveguide was 5–6 μm, the length of the samples was about 400 μm, the facets of the laser structures had no additional coatings.

Figure 4 presents typical light–current characteristics of two experimental structures with standard waveguides. The threshold current was about 11 mA, the differential efficiency being rather high. The output power could achieve 20 mW for the current amplitude of about 50 mA. The lasing wavelength was 838 nm at a current of 35 mA and the temperature of the active region of 15 °C. The optical spectrum was single-mode at currents up to 53 mA, its FWHM not exceeding 0.2 nm.

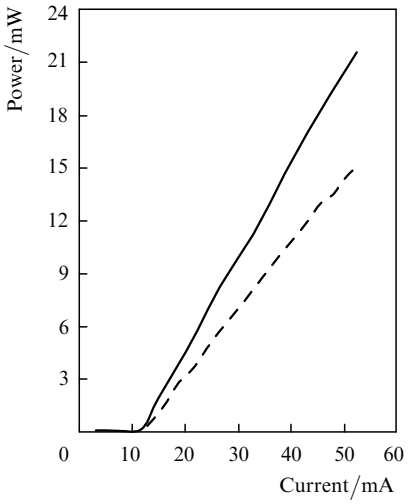

Figure 4. Light–current characteristics of two AQW lasers in the cw lasing regime.

However, when the laser waveguide stripe was inclined to the facets of the crystal, the emission characteristics changed strongly. The behaviour of the structure with the inclined stripe corresponds to a superluminescent diode rather than to a laser. Indeed, the light–current characteristic changed considerably (Fig. 5), while the width of the optical spectrum of the structure strongly increased (up to the 51.2-nm FWHM) and the spectrum had no peaks corresponding to the longitudinal modes of the laser

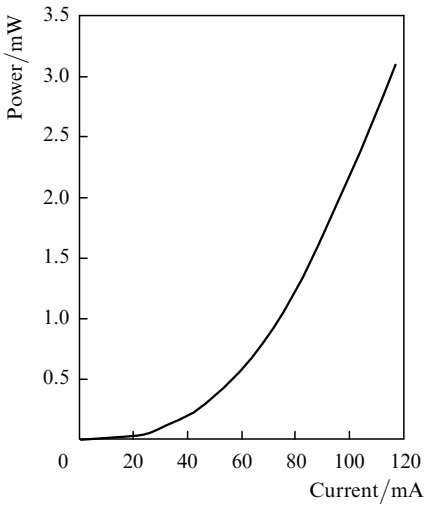

Figure 5. Typical light–current characteristic of a structure with an inclined stripe.

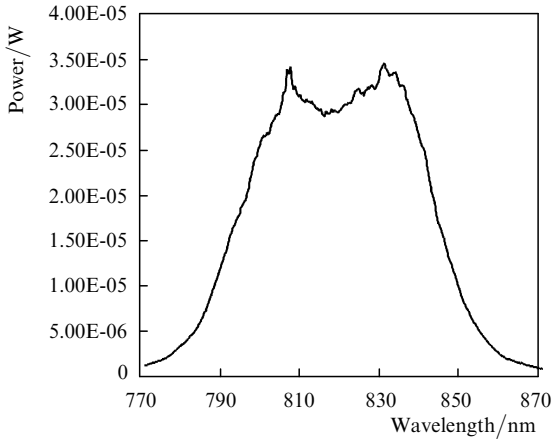

Figure 6. Ultimately broad optical emission spectrum of the AQW structure with an inclined stripe consisting of two QWs.

(Fig. 6). The width of the spectrum depends on the pump current. This dependence for another structure is shown in Fig. 7. The typical bandwidth exceeds 25 nm and its maximum value of 42.2 nm is achieved at a current of 54 mA. These values are consistent with the values calculated for AQW structures presented in Section 2 (see Fig. 3).

A large emission bandwidth of AQW structures provides tuning of laser radiation in a broad spectral range and can also ensure, in principle, the generation of short pulses.

We performed experiments on laser emission tuning. A laser structure emitting nearly flat-top spectrum (Fig. 6) was

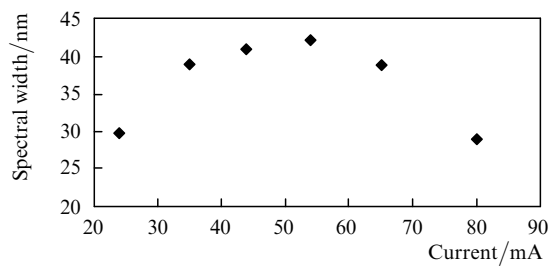

Figure 7. Emission spectrum bandwidth of an AQW structure as a function of the pump current.

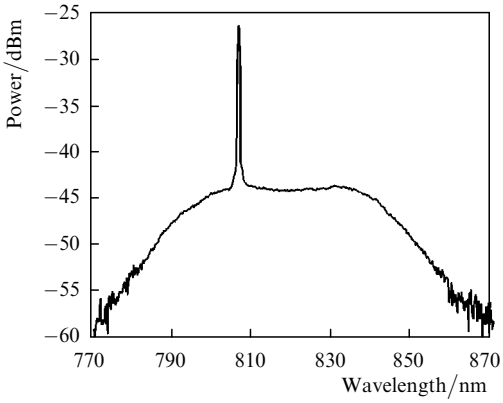

Figure 8. Typical emission spectrum of the laser with an external dispersion cavity in the cw lasing regime.

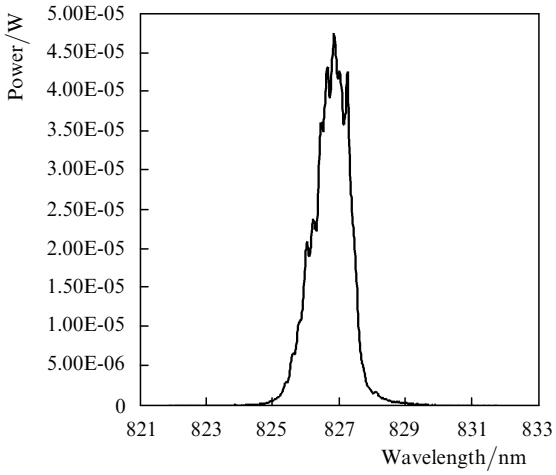

Figure 9. Emission spectrum in active mode locking regime of the laser with an external dispersion cavity.

placed in an external dispersive cavity with a configuration similar to that in [16]. A 600-line mm^{-1} diffraction grating served as an external reflector. When the external cavity was thoroughly adjusted, the laser generated the single-frequency emission with the linewidth of < 0.1 nm which could be tuned from 800 to 840 nm. The emission spectrum in this regime is shown in Fig. 8.

By changing the composition of the active layer, i.e. by varying the content x of aluminium in the heterostructure layers, it is possible to change the laser line wavelength and perform tuning in a broad spectral range. Such a source of tunable emission can be used in the near-IR spectroscopy.

4. Active mode locking

The generation of ultrashort pulses in AQW lasers has been achieved by using the simplest method of active mode locking [1]. A laser chip with an inclined stripe and a broad emission spectrum was placed into an external cavity consisting of a collimating objective and an external reflector. Either a plane highly reflecting mirror or a diffraction grating, as in the previous section, were used as the external reflector. The external cavity length was about 37.5 cm, which corresponded to the resonance modulation frequency of $\sim$400 MHz. This modulation frequency was chosen because the duration of generated pulses was also measured with a synchroscan streak camera with a temporal resolution of 10 ps. The camera operated at the resonance frequency of 100 MHz. Thus, it was possible to synchronise the camera sweep with the repetition rate of the emission pulses by dividing the modulation frequency by four.

A high-frequency sine-wave signal of power up to 1 W (30 dBm) was applied together with a direct current to the laser. To prevent overheating, the laser chip was mounted on a Peltie cooler. The temperature of the laser was kept equal to 15 °C by a thermal stabilisation system.

In addition to the synchroscan streak camera, the duration of pulses was measured by a standard autocorrelation method based on second harmonic generation. In this case, the accuracy of pulse duration measurement was better than 500 fs, which is much better than the temporal resolution of the camera.

The single-frequency emission spectrum of the laser in the external resonator drastically changed when the RF modulation was applied to the laser. The spectrum of the actively mode-locked laser (the modulation frequency is equal to the resonance frequency of the external resonator) is shown in Fig. 9. The width of the spectrum is 1.0 nm and the central wavelength is 827 nm. The direct pump current is 27 mA and the RF power is 1 W at the modulation frequency of 402.0 MHz. The output optical power in the mode locking regime was 4.7 mW.

Pulse duration measurements using the synchroscan streak camera showed that the measured pulse duration was ($\sim$10 ps) close to the time resolution of the camera. Therefore, accurate measurements of the pulse duration in experiments were performed by the method of intensity autocorrelation functions. Figure 10 presents a typical SHG autocorrelation function of mode-locked pulses. The FWHM of the SHG trace is 3.7 ps, which corresponds to the actual pulse duration of 2.4 ps assuming that the pulse envelope is described by hyperbolic secant [1].

Even shorter pulses were produced after the readjusting the cavity, a slight change in its length and the corresponding tuning of the resonance modulation frequency.

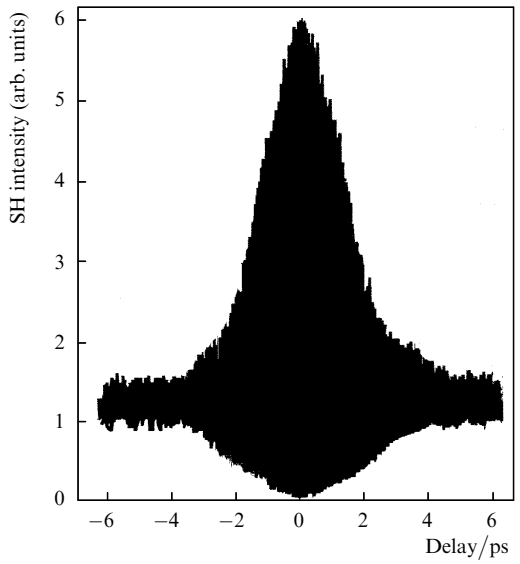

Figure 10. Fringe-resolved intensity autocorrelation function in the active mode-locking regime. The pulse duration is 2.4 ps.

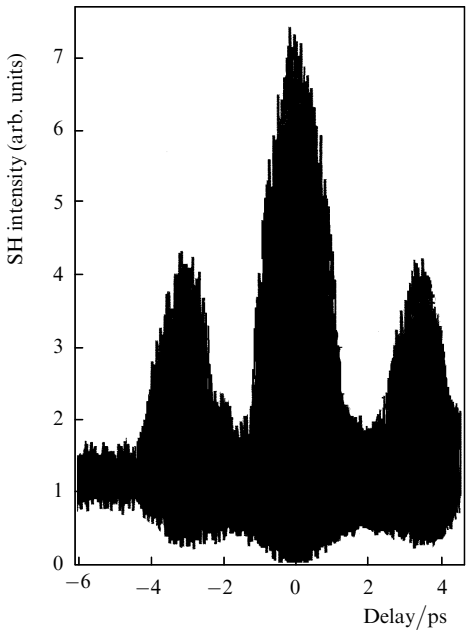

Figure 11. Same as in Fig. 10 but for different adjustment of the cavity. The duration of the main pulse is 1.2 ps.

Figure 11 illustrates the intensity autocorrelation function in this case. One can see that in addition to the central peak, the function has side peaks, which correspond to the presence of a subpulse. The subpulse is located at a distance of about 3.4 ps from the main pulse. The main pulse duration is 1.2 ps. Such a pulse compression compared to the single pulse duration (2.4 ps) can be caused by the pulse collision effect in a nonlinear medium [1, 17].

The central frequency of the spectrum of mode-locked pulses can be varied by changing the position of the diffraction grating. In this case, the emission spectrum looked similarly to that presented in Fig. 8. The duration of the emission pulses remained almost the same within the entire tuning range from 800 to 840 nm except the boundaries of this range. It was possible to generate picosecond pulses with a repetition rate up to 1 GHz by changing the external cavity length and adjusting properly the modulation frequency.

Experiments on active mode locking have shown that modes can be excited and locked only in a small region (about 1 nm) of the whole spectral range (30 – 40 nm) corresponding to the gain bandwidth of the semiconductor medium. This is explained, in our opinion, by the following fact. The shortening of the pulse duration and the corresponding broadening of the spectrum in the mode locking regime is caused by a stronger amplification per each round trip in the cavity of a part of the pulse lying near the maximum of the gain. The other parts of the pulse either are amplified weaker or even absorbed due to the modulation of the gain by the external signal. Because the modulation period lies in nanosecond range, the curvature of the time dependence of the gain is small on time intervals corresponding to the pulse duration. Therefore, the pulse shortening in the picosecond range only due to the resonance modulation of the gain becomes negligible. This means in the frequency domain that the spectral bandwidth where the external cavity modes are locked, remains quite narrow. In other words, the efficiency of pure active mode locking is not enough for the generation of pulses of duration less than 1 ps. To generate shorter pulses and to use the entire available gain bandwidth of AQW lasers, it is necessary to realise hybrid active/passive mode locking by using saturable absorbers. This will be done in our future work.

Note in conclusion that the third-order (Kerr type) nonlinearity of the active medium of lasers can affect substantially their dynamics. This nonlinearity in semiconductor lasers is manifested due to a strong dependence of the refractive index on the carrier density and belongs to giant nonlinearities [18]. Therefore, a special attention should be paid in the future to the use of the Kerr nonlinearity in semiconductor lasers for enhancing mode locking and generating even shorter optical pulses.

5. Conclusions

We have performed the experimental and theoretical study of AQW lasers. The theoretical model of the optical gain in lasers with an arbitrary number of quantum wells of arbitrary widths and compositions has been developed. The optical gain spectra have been calculated for lasers with two and four QWs. It has been shown theoretically that the gain bandwidth of AQW structures can achieve 30 – 40 nm, which exceeds by several times the corresponding bandwidth of standard QW lasers. It has been demonstrated that it is possible to fabricate an AQW structure with a broad and nearly flat-top spectrum by a careful selection of parameters, which is important both for the development of narrowband tunable lasers and generation of ultrashort pulses.

The first experimental samples of AQW structures for the generation of ultrashort pulses have been fabricated. A structure with two QWs having different widths has been calculated and its optimum parameters providing the maximum emission bandwidth have been determined. The experimental study of the fabricated samples of lasers and superluminescent diodes has demonstrated good agreement between experimental and calculated parameters. The experimental emission bandwidth was 30 – 40 nm, which is a promising result. A narrowband (< 0.1 nm) radiation source tunable in the wavelength range from 800 to 840 nm has been fabricated.

Active mode locking has been performed in an AQW laser with an external dispersion cavity. Tunable optical pulses with duration of 1 – 2 ps at a repetition rate of about 400 MHz have been obtained. Similar AQW structures are promising for the realisation of hybrid active/passive mode locking with the help of saturable absorbers, which will provide the generation of shorter and more powerful pulses with duration of several hundred femtoseconds.

Acknowledgements. The authors thank Yu.V. Korzhetsky for his help in numerical calculations. This work was partially supported by the Russian Foundation for Basic Research (Grant No. 06-02-16173a) and the President Grant for Leading Scientific Schools (Grant No. NS-6055.2006.2).

References

1. Vasil'ev P. *Ultrafast Diode Lasers: Fundamentals and Applications* (Norwood: Artech House, 1995).

2. Ikeda S., Shimizu A., Hara T. *Appl. Phys. Lett.*, **55**, 1155 (1989).
3. Gingrich H.S., Chummey D.R., Sun S.-Z., Hersee S.D., Lester L.F., Brueck S.R.J. *IEEE Photon. Tech. Lett.*, **9**, 155 (1997).
4. Lee B.-L., Lin C.-F. *IEEE Photon. Tech. Lett.*, **10**, 322 (1998).
5. Kononenko V.K., Afonenko A.A., Manak I.S., Nalivko S.V. *Opto-Electronics Review*, **8**, 241 (2000).
6. Kwon O.K., Kim K.H., Sim E.D., Kim J.H., Kim H.S., Oh K.R. *IEEE Photon. Tech. Lett.*, **17**, 537 (2005).
7. Woodworth S.C., Cassidy D.T., Hamp M.J. *IEEE J. Quantum Electron.*, **39**, 426 (2003).
8. Brennan M.J., Milgram J.N., Mascher P., Haugen H.K. *Appl. Phys. Lett.*, **81**, 2502 (2002).
9. Kononenko V.K., Manak I.S., Nalivko S.V., Shvetsov V.A., Shuljaev D.S. *J. Applied Spectr.*, **64**, 221 (1997).
10. Hamp M.J., Cassidy D.T. *IEEE J. Quantum Electron.*, **36**, 978 (2000).
11. Hamp M.J., Cassidy D.T. *IEEE J. Quantum Electron.*, **37**, 92 (2001).
12. Vandermeer A.D., Cassidy D.T. *IEEE J. Quantum Electron.*, **41**, 917 (2005).
13. Makino T. *IEEE J. Quantum Electron.*, **32**, 493 (1996).
14. Zory P.S. (Ed.) *Quantum Well Lasers* (New York: Academic Press, 1993).
15. Rosenzweig M., Mohrle M., Duser H., Venghaus H. *IEEE J. Quantum Electron.*, **27**, 1804 (1991).
16. Bessonov Yu.L., Bogatov A.P., Vasil'ev P.P., et al. *Kvantovaya Elektron.*, **9**, 2323 (1982) [*Sov. J. Quantum Electron.*, **12**, 1510 (1982)].
17. Vasil'ev P.P., Morozov V.N., Popov Yu.M., Sergeev A.B. *IEEE J. Quantum Electron.*, **22**, 149 (1986).
18. Bogatov A.P., Duraev V.P., Eliseev P.G., Luk'janov S.A. *Kvantovaya Elektron.*, **15**, 1552 (1988) [*Sov. J. Quantum Electron.*, **18**, 971 (1988)].